Second-Order Perturbational Effect on the Interlayer Interactions in Graphite and Graphite Intercalation Compounds

Kazunari Yoshizawa,* Takashi Kato, and Tokio Yamabe

Department of Molecular Engineering, Kyoto University, Sakyo-ku, Kyoto 606-8501

Institute for Fundamental Chemistry, 34-4 Takano-Nishihiraki-cho, Sakyo-ku, Kyoto 606-8103

(Received March 30, 1998)

The role of second-order perturbations in interlayer interactions of two-dimensional electronic systems is examined from simple two-layer models. The preferred nuclear motions are discussed specifically for the preferred stacking of layers in graphite on the basis of transition-density analyses for extended systems. The well-known *ABAB* stacking of layers in neutral graphite and the *AAAA* stacking of layers in graphite intercalation compounds (GICs) such as C_6Li and C_8K complexes are proposed to be consequences of orbital interactions (near the Fermi level) between nearest neighbor layers. This paper raises doubts about a widely accepted belief that the interlayer interaction between graphite layers is of the van der Waals type.

Diamond and graphite are strikingly different.[1] In diamond, each carbon atom forms single bonds with four adjacent carbon atoms at the corners of a regular tetrahedron. As a result, its tightly bonded three-dimensional network forms the hardest known substance. On the other hand, graphite consists of two-dimensional layers in which each carbon atom has three nearest neighbor carbon atoms. A single layer of graphite has honeycomb hexagons formed by three sp^2 hybridized orbitals of carbon. Each graphite layer is quite slippery so that graphite is often used as a solid lubricant. Graphite is now of great technological importance as a moderator in nuclear reactors, a reinforcement fiber in various composite materials, and a cathode material in lithium ion rechargeable battery.

The most common form of natural graphite consists of the *ABAB* stacking of layers (so-called Bernal structure),[2] as shown in Scheme 1, in which the closed and open circles are crystallographically equivalent carbon atoms. The in-plane C–C bond length is 1.42 Å and the interlayer separation is 3.35 Å. From our calculations, the in-plane nearest-neighbor $p\pi$ overlap is 0.24 and the interlayer nearest neighbor $p\sigma$ overlap is 0.03. The interlayer orbital interactions are thus weak compared with those within a layer, but not negligible. Although most textbooks of inorganic chemistry[1] state that the graphite layers are held together by van der Waals forces, there are non-negligible orbital interactions between nearest neighbor layers, as sometimes suggested.[3]

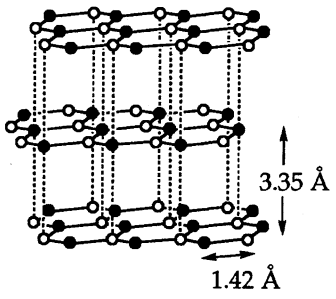

Scheme 1.

The rhombohedral structure of graphite has the *ABC* stacking of layers.[2] In this structure, the equivalent planes appear every third layer in the direction of the *c* axis that is vertical to graphite planes. The *ABC* stacking mode is always contained together with the *ABAB* stacking mode in natural and synthetic graphite. This stacking mode is supposed to be a slight modification of the common *ABAB* stacking mode from the point of view of interactions between nearest neighbor layers. The fact that the *ABAB* stacking mode is more common than the *ABC* stacking mode suggests that there are still unknown interactions between distant layers.

The third form of graphite has an *AAAA* stacking of layers.[2] Although this stacking mode is not observed in natural and synthetic graphite, it occurs generally in graphite intercalation compounds (GICs) such as C_6Li and C_8K complexes.[2] Both the C_6Li and C_8K complexes are the so-called stage-1 GICs, in which a layer of alkali metals is present between each pair of graphite layers. The interlayer separations in C_6Li and C_8K are 3.71 and 5.41 Å, respectively. Three-dimensional band structures of the above-mentioned three types of stacking modes in graphite, i.e., *ABAB*, *ABC*, and *AAAA*, were calculated by McClure[4] and by Samuelson et al.[5]

The purpose of this paper is to investigate the electronic consequences of interlayer interactions on structural changes in two-dimensional extended systems. We discuss specifically the interlayer interactions in graphite and GICs in terms of second-order perturbation theory.[6—8] We show how orbital interactions contribute to the formations of the *ABAB* stack-

ing mode in graphite and of the *AAAA* stacking mode in GICs.

Second-Order Perturbations in Extended Systems

The Peierls distortion,[9] the indication that a regular chain structure is potentially unstable in a one-dimensional electronic system with a partially filled band, is the solid state analogue of the Jahn–Teller effect. Distortion of one-dimensional chains takes place through coupling between an electronic state and a phonon, a normal mode of vibration of the underlying lattice that can drive the structure into an electronically more favorable configuration.[10—14] This type of distortion in one-dimensional systems leads to an important metal-insulator transition. This is a famous first-order effect in extended systems.

Linear chain distortion as a consequence of interchain interactions can be classified as a second-order effect in extended systems.[15] Several examples of second-order distortion are known so far in interesting solid systems.[16—19] Useful discussions of intra- and interchain interactions in one-dimensional solids, analyzed in terms of orbital interactions, is found in Whangbo's articles.[15,20] A method of moments has been proposed by Burdett and Mitchell[21] to study the electronic driving force for disorder-to-order transitions in low-dimensional solids. Moreover, Aoki and Imamura[22] showed analytically that interchain interactions suppress the bond-length alternation in a polyene chain.

According to Bader[23] and Pearson,[24] a transition force operates on nuclei along a certain normal coordinate when a transition density has the same symmetry as displacement of atoms from equilibrium nuclear positions. This is one of the most important concepts in the so-called orbital symmetry rules[6—8] for chemical reactions in molecular systems. This concept was applied first by Yoshizawa and Hoffmann[25] to the interchain interactions in infinite electronic systems. In previous papers, we have shown that a second-order term originating from two different bands near the Fermi level leads to favorable motions of nuclei in extended systems.[25,26] Such orbital interactions in extended systems are found to play an important role in the determination of one-dimensional interchain and two-dimensional interlayer couplings. It appeared that preferred nuclear motion in interchain and interlayer problems can be predicted from analyses of transition density between two bands in the vicinity of the Fermi level. For example, there appears an out-of-phase coupling of off-diagonal CDWs (charge density waves) on neighbor chains, as shown in Scheme 2.[25] The arrows in this illustration are transition forces, or preferred nuclear motions. This is an interesting second-order effect in infinite one-dimensional systems. Our transition-density analysis is, of course, fully consistent with Whangbo's analysis.[15]

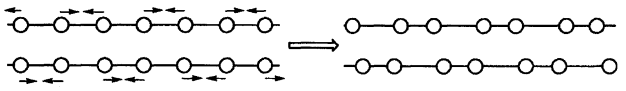

Scheme 2.

Detailed formulations for the second-order effects in infinite one- and two-dimensional systems are seen in previous papers.[25,26] It is likely to be quite interesting to consider systematically the interlayer interactions and possible stacking modes in graphite and GICs from a point of view of transition-density analysis. A part of the analyses of the *ABAB* stacking mode in neutral graphite can be found in Ref. 26.

ABAB Stacking of Layers in Graphite

Although the graphite layers are described as being held together by van der Waals forces,[1] to the best of our knowledge detailed theoretical analysis on the interlayer interactions has not yet been performed. There are non-negligible orbital interactions between the two layers of graphite. Although the interlayer interactions are small, they cause a band overlap that is responsible for the semimetallic properties of graphite. The interlayer orbital interactions are weak compared with those within a layer, but not negligible. Interlayer orbital interactions for the graphite-to-diamond high-pressure reaction were analyzed by Kertesz and Hoffmann.[27] General features of orbital interactions in graphite are seen in Lowe's textbook.[28]

Let us first consider a simple two-layer *AA* stacking model, shown in Scheme 3. There are four carbons per unit cell in this two-layer model. Each carbon has one electron in each pπ orbital, so that there are totally four π electrons per unit cell. The arrows a_1 and a_2 are lattice vectors defining the two-dimensional graphite network. From a quantum chemical viewpoint,[6—8] let us examine the second-order effects that might drive the structure into a different, more favorable configuration.

According to Bloch's theorem,[29] the tight-binding wave function (crystal orbital) can be written as Eq. 1:

$$|k_1,k_2,l\rangle = \frac{1}{\sqrt{N}}\sum_{\nu_1}\sum_{\nu_2}\sum_{\mu} e^{i(k_1\nu_1 a_1 + k_2\nu_2 a_2)} \times c_{k_1,k_2,l,\mu}\,\phi_\mu(x_1,-\nu_1 a_1, x_2-\nu_2 a_2), \quad (1)$$

where k_1 and k_2 are the wave vectors; l the band index; $\phi_\mu(x_1-\nu_1 a_1, x_2-\nu_2 a_2)$ the μth atomic orbital at the cell (ν_1, ν_2); N the total number of the cells; and $c_{k_1,k_2,l,\mu}$ the expansion coefficient.

Since the nearest-neighbor pπ overlap within a layer is greater than the pσ overlap between nearest neighbor layers, we can write by orbital symmetry[30] the crystal orbitals of the four π bands as Eqs. 2, 3, 4, and 5, respectively.

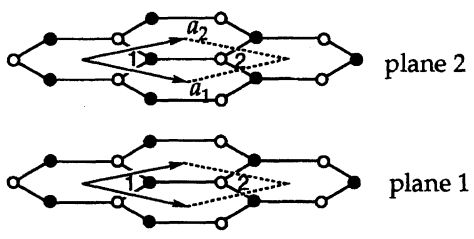

Scheme 3.

$$|k_1,k_2,1\rangle = \frac{1}{\sqrt{N}}\sum_{\nu_1}\sum_{\nu_2} e^{i(k_1\nu_1a_1+k_2\nu_2a_2)}\{\phi_{1,1}(x_1-\nu_1a_1,\ x_2-\nu_2a_2) + \phi_{1,2}(x_1-\nu_1a_1,\ x_2-\nu_2a_2) - \phi_{2,1}(x_1-\nu_1a_1,\ x_2-\nu_2a_2) - \phi_{2,2}(x_1-\nu_1a_1,\ x_2-\nu_2a_2)\}, \quad (2)$$

$$|k_1,k_2,2\rangle = \frac{1}{\sqrt{N}}\sum_{\nu_1}\sum_{\nu_2} e^{i(k_1\nu_1a_1+k_2\nu_2a_2)}\{\phi_{1,1}(x_1-\nu_1a_1,\ x_2-\nu_2a_2) + \phi_{1,2}(x_1-\nu_1a_1,\ x_2-\nu_2a_2) + \phi_{2,1}(x_1-\nu_1a_1,\ x_2-\nu_2a_2) + \phi_{2,2}(x_1-\nu_1a_1,\ x_2-\nu_2a_2)\}, \quad (3)$$

$$|k_1,k_2,3\rangle = \frac{1}{\sqrt{N}}\sum_{\nu_1}\sum_{\nu_2} e^{i(k_1\nu_1a_1+k_2\nu_2a_2)}\{\phi_{1,1}(x_1-\nu_1a_1,\ x_2-\nu_2a_2) - \phi_{1,2}(x_1-\nu_1a_1,\ x_2-\nu_2a_2) - \phi_{2,1}(x_1-\nu_1a_1,\ x_2-\nu_2a_2) + \phi_{2,2}(x_1-\nu_1a_1,\ x_2-\nu_2a_2)\}, \quad (4)$$

$$|k_1,k_2,4\rangle = \frac{1}{\sqrt{N}}\sum_{\nu_1}\sum_{\nu_2} e^{i(k_1\nu_1a_1+k_2\nu_2a_2)}\{\phi_{1,1}(x_1-\nu_1a_1,\ x_2-\nu_2a_2) - \phi_{1,2}(x_1-\nu_1a_1,\ x_2-\nu_2a_2) + \phi_{2,1}(x_1-\nu_1a_1,\ x_2-\nu_2a_2) - \phi_{2,2}(x_1-\nu_1a_1,\ x_2-\nu_2a_2)\}. \quad (5)$$

Here $\phi_{2,1}(x_1-\nu_1a_1,\ x_2-\nu_2a_2)$ is the atomic orbital on site 1 of plane 2 in the cell $(\nu_1,\ \nu_2)$, for example. These are a qualitative description of the four π bands for the two layer model of graphite. The energy of band 1 is found from orbital symmetry to be the lowest and that of band 4 to be the highest at point $\Gamma = (0, 0)$.

Figure 1 shows the π band structure near the Fermi level for the two-layer *AA* stacking model calculated with the extended Hückel method.[31] A 200 *k*-point set along a symmetry line was used for band structure calculations; 55 mesh-points in the irreducible part of the Brillouin zone were generated according to Ramirez and Böhm[32] for calculations of density of states (DOS). Lattice sums for band structure calculations were taken to the fifth-nearest neighbors. The shaded area in the DOS indicates the contribution from the π bands, and the dotted line marks the Fermi level. The splitting of the two bands is a measure of the strength of the interlayer interaction. When the interaction is weak, the splitting is small. So the reader can find only two σ bands in Fig. 1, although there are actually four σ bands.

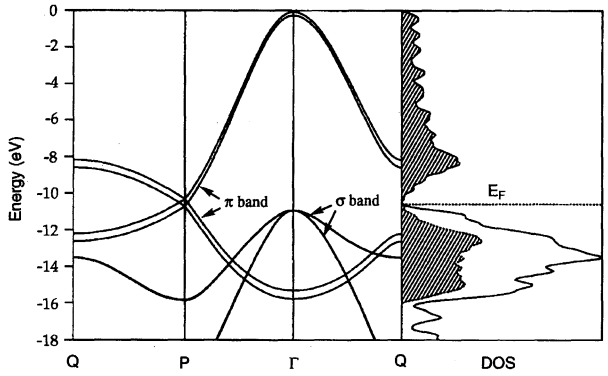

Fig. 1. Band structure of a two-layer *AA* stacking model of graphite. The dotted line marks the Fermi level; and the shaded area in the DOS indicates the contribution of π-bands.

The two level crossings of the bands 1 and 3 and the bands 2 and 4 occur at an important symmetry point P = $(4\pi/3a_1,\ 2\pi/3a_2)$, as schematically shown in Scheme 4. Let us look at these level crossings. The closed and open circles in this illustration indicate occupied and unoccupied levels. It is quite clear from the second-order perturbation theory that the mixing of the levels near the Fermi energy dominates the energy stabilization. The well-established frontier orbital theory[7] and Woodward–Hoffmann rules[6] are based on the second-order perturbation theory.

We think a second-order effect that results from occupied and unoccupied bands at point P should be very important for the interlayer interactions in graphite. Without losing generality, we can take a linear combination of orbitals at a degenerate point in order to get an equivalent, more useful representation. We thus obtain Eqs. 6 and 7 from linear combinations of the occupied bands 1 and 3 at point P.

$$|4\pi/(3a_1),2\pi/(3a_2),1'\rangle = \frac{|4\pi/(3a_1),2\pi/(3a_2),1\rangle + |4\pi/(3a_1),2\pi/(3a_2),3\rangle}{2} = \frac{1}{\sqrt{N}}\sum_{\nu_1}\sum_{\nu_2}\exp\left\{i\left(\frac{4}{3}\pi\nu_1+\frac{2}{3}\pi\nu_2\right)\right\} \times\{\phi_{1,1}(x_1-\nu_1a_1,\ x_2-\nu_2a_2) - \phi_{2,1}(x_1-\nu_1a_1,\ x_2-\nu_2a_2)\}, \quad (6)$$

$$|4\pi/(3a_1),2\pi/(3a_2),2'\rangle = \frac{|4\pi/(3a_1),2\pi/(3a_2),1\rangle - |4\pi/(3a_1),2\pi/(3a_2),3\rangle}{2} = \frac{1}{\sqrt{N}}\sum_{\nu_1}\sum_{\nu_2}\exp\left\{i\left(\frac{4}{3}\pi\nu_1+\frac{2}{3}\pi\nu_2\right)\right\} \times\{\phi_{1,2}(x_1-\nu_1a_1,\ x_2-\nu_2a_2) - \phi_{2,2}(x_1-\nu_1a_1,\ x_2-\nu_2a_2)\}. \quad (7)$$

We can also take linear combinations of the crystal orbitals of unoccupied bands 2 and 4 at point P to get a useful pair of crystal orbitals.

$$|4\pi/(3a_1),2\pi/(3a_2),3'\rangle = \frac{|4\pi/(3a_1),2\pi/(3a_2),2\rangle + |4\pi/(3a_1),2\pi/(3a_2),4\rangle}{2} = \frac{1}{\sqrt{N}}\sum_{\nu_1}\sum_{\nu_2}\exp\left\{i\left(\frac{4}{3}\pi\nu_1+\frac{2}{3}\pi\nu_2\right)\right\} \times\{\phi_{1,1}(x_1-\nu_1a_1,\ x_2-\nu_2a_2) + \phi_{2,1}(x_1-\nu_1a_1,\ x_2-\nu_2a_2)\}, \quad (8)$$

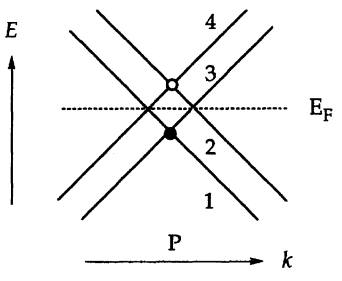

Scheme 4.

$$|4\pi/(3a_1), 2\pi/(3a_2), 4'\rangle$$
$$= \frac{|4\pi/(3a_1), 2\pi/(3a_2), 2\rangle - |4\pi/(3a_1), 2\pi/(3a_2), 4\rangle}{2}$$
$$= \frac{1}{\sqrt{N}} \sum_{\nu_1} \sum_{\nu_2} \exp\left\{ i \left(\frac{4}{3}\pi\nu_1 + \frac{2}{3}\pi\nu_2 \right) \right\}$$
$$\times \{ \phi_{1,2}(x_1 - \nu_1 a_1,\ x_2 - \nu_2 a_2) + \phi_{2,2}(x_1 - \nu_1 a_1,\ x_2 - \nu_2 a_2) \}. \quad (9)$$

In Fig. 2, we show schematic representations of the crystal orbitals at the closed and open circles (in Scheme 4) that correspond to Eqs. 6 and 9, respectively. These orbitals are clearly of a nonbonding nature within a single layer. It is essential to note that the occupied one (Eq. 6) is in-phase between the two layers and the unoccupied one (Eq. 9) is out-of-phase.

The *AA* stacking model is not appropriate for neutral graphite, as mentioned above. We take a look at the second-order effects that can drive the *AA* stacking mode into a different, more favorable configuration. It is important to consider relaxation of electron distributions through the mixing between the occupied and unoccupied levels in the vicinity of the Fermi energy. To predict a preferred stacking of layers, let us now calculate the transition density at the occupied and unoccupied points near the Fermi level. Collecting a few terms on the assumption of a nearest-neighbor approximation, we finally obtain complicated Eqs. 10 and 11.

$$\langle 4\pi/(3a_1), 2\pi/(3a_2), 1' | \sum_j \delta(r - r_j) | 4\pi/(3a_1)$$
$$+Q_1, 2\pi/(3a_2) + Q_2, 4' \rangle$$
$$= \frac{1}{N} \sum_{\nu_1} \sum_{\nu_2} [\exp(iQ_1 a_1 \nu_1 + iQ_2 a_2 \nu_2)$$
$$\times \{ (\alpha_{1112} + \alpha_{1122} - \alpha_{2112} - \alpha_{2122})$$
$$+\exp\left(-i\frac{4\pi}{3}\right)(\beta_{1112} + \beta_{1122} - \beta_{2112} - \beta_{2122})$$
$$+\exp\left(-i\frac{2\pi}{3}\right)(\gamma_{1112} + \gamma_{1122} - \gamma_{2112} - \gamma_{2122})\}], \quad (10)$$

$$\langle 4\pi/(3a_1), 2\pi/(3a_2), 3' | \sum_j \delta(r - r_j) | 4\pi/(3a_1)$$
$$+Q_1, 2\pi/(3a_2) + Q_2, 2' \rangle$$
$$= \frac{1}{N} \sum_{\nu_1} \sum_{\nu_2} [\exp(iQ_1 a_1 \nu_1 + iQ_2 a_2 \nu_2)$$
$$\times \{ (\alpha_{1112} - \alpha_{1122} + \alpha_{2112} - \alpha_{2122})$$
$$+\exp\left(-i\frac{4\pi}{3}\right)(\beta_{1112} - \beta_{1122} + \beta_{2112} - \beta_{2122})$$
$$+\exp\left(-i\frac{2\pi}{3}\right)(\gamma_{1112} - \gamma_{1122} + \gamma_{2112} - \gamma_{2122})\}], \quad (11)$$

where Q_1 and Q_2 are wave-vector parameters, and

$$\alpha_{ijkl} = \phi_{i,j}(x_1 - \nu_1 a_1,\ x_2 - \nu_2 a_2)\phi_{k,l}(x_1 - \nu_1 a_1,\ x_2 - \nu_2 a_2)$$

is the intracell overlap within a plane ($i = k$) and between layers ($i \neq k$). Moreover,

$$\beta_{ijkl} = \phi_{i,j}(x_1 - (\nu_1 + 1)a_1,\ x_2 - \nu_2 a_2)\phi_{k,l}(x_1 - \nu_1 a_1,\ x_2 - \nu_2 a_2)$$

and

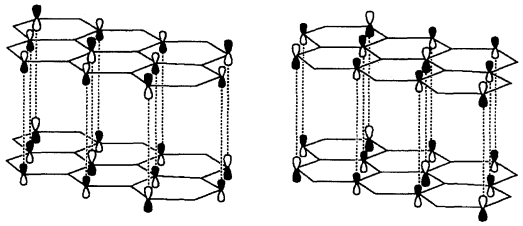

Fig. 2. Crystal orbitals, Eq. 6 (left) and Eq. 9 (right), for a two-layer *AA* stacking model of graphite at point P. The left one is filled and the right one unfilled.

$$\gamma_{ijkl} = \phi_{i,j}(x_1 - \nu_1 a_1,\ x_2 - (\nu_2 + 1)a_2)\phi_{k,l}(x_1 - \nu_1 a_1,\ x_2 - \nu_2 a_2)$$
$$(i, j, k, l = 1 \text{ or } 2)$$

are the corresponding nearest-neighbor intercell overlaps. For example, α_{1122} is the intracell overlap between site 1 of plane 1 and site 2 of plane 2; β_{1122} and γ_{1122} are the intercell overlap between site 1 of plane 1 and site 2 of plane 2; and so on. In order to help our understanding, these interactions are schematically indicated in Scheme 5. These are off-diagonal densities that can cause preferred deformation.

Now we are interested in the off-diagonal densities in these equations, since off-diagonal terms are the driving force for atomic displacements. As mentioned above, interchain off-diagonal densities should lead to an important occurrence of out-of-phase coupling of CDWs on neighbor chains in one-dimensional systems.[25] Thus, let us focus our attention on the analysis of the interlayer off-diagonal part of the transition density of Eqs. 10 and 11. We will show that a certain layered structure distorted from the original *AA* stacking mode should be stabilized through a particular nuclear motion.

We take $Q_1 = Q_2 = 0$ into account in Eqs. 10 and 11. This is because the unit cell of a single graphite layer contains two carbon atoms and, as a consequence, two bands crossing at point P are considered to come from a single band that is folded back at this point. As mentioned in the previous section, the transition force operates on the nuclei when the transition density and the displacement of the atoms from the equilibrium nuclear positions along a normal coordinate have the same symmetry. In order to predict the distortion that is favored as a result of interlayer interaction, we examine the shape of the transition density using a diagram.

We show schematically in Scheme 6 how the transition density favors the nuclear motion of graphite layers with the same symmetry as the transition density. This illustration corresponds to the transition density of Eq. 10. Here circled "+" and "−" represent the signs of the product of neighbor

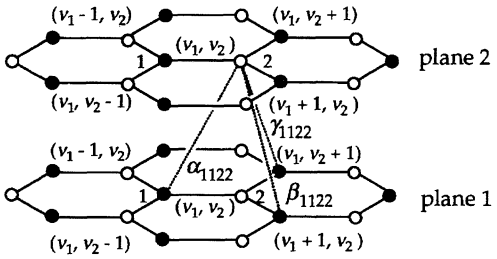

Scheme 5.

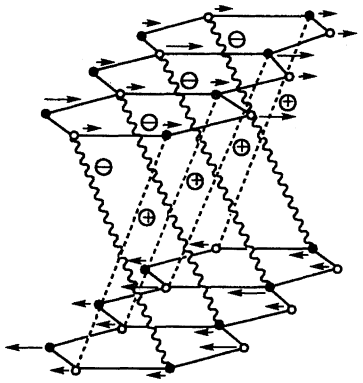

Scheme 6.

orbitals, α_{ijkl}, β_{ijkl}, and γ_{ijkl}, mentioned above in Scheme 5.

Note that "+" and "−" signify out-of-phase and in-phase combinations between p orbitals of the neighbor layers, respectively, because the p orbital is antisymmetric in respect of its nodal plane. Therefore the wavy and broken lines in Scheme 6 indicate attractive and repulsive forces, respectively, according to the perturbational analysis of Bader.[23] From the illustration of this transition density, we understand that the charge is displaced from the "+" region to the "−" region as a consequence of the slide of the layers. Thus, the vectors in Scheme 6 show the forces acting on the nuclei, or their preferred motion, due to the electron-distribution relaxation. It is reasonable to presume that the positively charged nuclei should move in the direction of increased electron density. Consequently, the two graphite layers slightly slide from the original *AA* stacking mode, as shown in Scheme 7.

The vectors in Scheme 7 show the preferred motion of the layers, due to the electron-distribution relaxation. The deformed structure shows the resultant *AB* stacking. This sliding of layers is a direct consequence of orbital interactions near the Fermi level, described by the transition density analysis for extended systems, indicated by Eq. 10. The other partner (Eq. 11) will cause the two layers to slide to the reverse direction; the resultant structure is the same.

The preferred sliding of layers shown above is caused by the interactions between the occupied and unoccupied levels in different bands at point P, as shown from the transition density analysis. The favorable form of stacking is consistent with the "largest overlap" principle; in fact, the overlap integral is the largest in the *AB* stacking. The level crossings at point P, shown in Fig. 1, are removed as a consequence of orbital mixing between different bands. This situation is quite different from the usual Peierls distortion where splittings are caused by the interactions in a single band, i.e., a first-order effect. Discussions about the distinction between

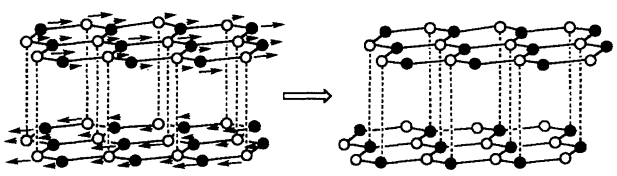

Scheme 7.

first- and second-order effects in extended systems can be found in Refs. 15, 16, 17, 18, 19, and 20. The band structure and DOS of the resultant *AB* stacking model are shown in Fig. 3.

The essential change in the vicinity of the Fermi level through this distortion is removal of the two degenerate points at P, as indicated in Scheme 8. Instead, a single-point degeneracy remains at the Fermi level. The fact that the band splitting in the *AB* stacking is small compared with that of the *AA* stacking indicates that the interlayer interaction in the *AB* stacking is smaller. Net energy stabilization by this preferred deformation is 0.02 eV per unit cell, from extended Hückel calculations. We do not discuss this energy difference anymore because the purpose of this paper is to gain a qualitative understanding; our *k*-point set in the irreducible part of the Brillouin zone is too small for quantitative analyses. In any case, this value is quite small, so that each graphite layer is slippery.

AAAA Stacking of Layers in Graphite Intercalation Compounds

Next we consider the reason why graphite intercalation compounds (GICs) take the *AAAA* stacking of layers.[2] Let us first look at the structure of the C_6Li complex. The crystal of C_6Li forms an alternating sequence of a carbon layer and a lithium layer, as shown in Scheme 9. The two-dimensional structure of a single layer of graphite and lithium is also shown in this illustration.

The triangular lattice arrangement of lithium atoms is re-

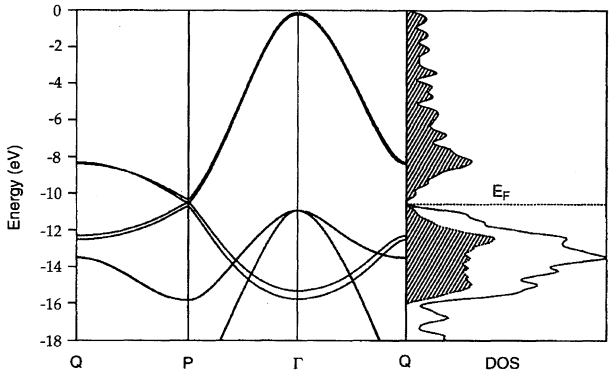

Fig. 3. Band structure of a two-layer *AB* stacking model of graphite. The dotted line marks the Fermi level; and the shaded area in the DOS indicates the contribution of π-bands.

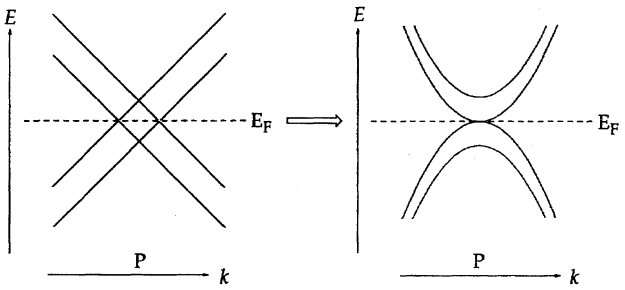

Scheme 8.

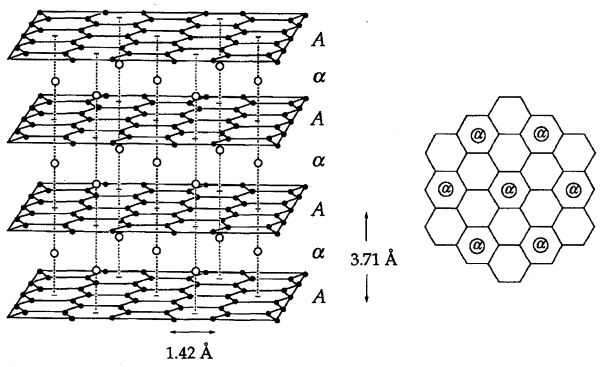

Scheme 9.

peated in every graphite layer. That is to say the stage-1 C_6Li complex consists of alternating carbon and lithium layers, whose layer stacking sequence is $A\alpha A\alpha\cdots$, where A denotes a carbon layer and α a lithium layer.[33—36] By lithium intercalation, the C–C bond length of 1.42 Å is not changed, but the distance between nearest neighbor graphite layers is pushed apart slightly from 3.35 to 3.71 Å. Although the interlayer nearest neighbor pσ overlap is diminished in the C_6Li complex, we think that there are still important orbital interactions between nearest neighbor layers, as well as coulomb interactions between graphite and lithium layers.

Let us next look at the structure of the C_8K complex.[2] The three-dimensional and two-dimensional structures of C_8K is shown in Scheme 10. From this illustration, we can see that there are four kinds of equivalent potassium layers along the c axis. The periodic arrangement of the potassium atoms is repeated in every fifth potassium layer along the c axis. Thus, the stage-1 C_8K complex consists of alternating carbon and potassium layers, whose layer stacking sequence is $A\alpha A\beta A\gamma A\delta A\alpha A\beta A\gamma A\delta\cdots$ where A denotes a carbon layer and α, β, γ, and δ denote a potassium layer.[37—39] By potassium intercalation, the C–C bond length within a layer is not significantly changed, being still approximately 1.42 Å. On the other hand, the distance between nearest neighbor carbon layers (5.41 Å) becomes much larger than those of neutral graphite and C_6Li, because the ionic radius of potassium (1.52 Å) is larger than that of lithium (0.90 Å). As

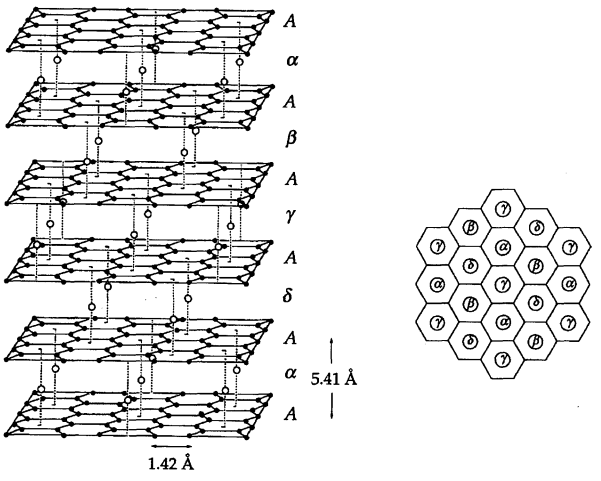

Scheme 10.

a consequence, the interlayer nearest neighbor pσ overlap is significantly decreased to 1/100 of that for neutral graphite.[40] However, we still believe that interlayer orbital interactions should play a role for the formation of the *AAAA* stacking mode in C_8K. As mentioned above, the fact that in neutral graphite the *ABAB* stacking mode is more common than the *ABC* stacking mode indicates that there are weak interactions between second-nearest-neighbor layers that are separated by 6.7 Å.

For the transition-density analyses for the interlayer interactions in GICs, it is essential to note that the Fermi level in GICs goes up compared with that of neutral graphite, due to electron doping. Let us next estimate the Fermi level change in GICs. In the C_6Li complex, each carbon has a net change of $-1/6$ so that four carbons in the unit cell of our two-layer model (Scheme 3) have a total net charge of $-2/3$. Also in the C_8K complex, each carbon has a net charge of $-1/8$, and four carbons in the unit cell have a net charge of $-1/2$. In this way, we can estimate the Fermi levels for these GICs by considering the DOS of Fig. 1. In the C_6Li complex, the Fermi level should go up in such a way that it divides the DOS of the π bands (indicated by the shaded area in Fig. 1) in the ratio 7 : 5, and it becomes approximately -8.5 eV in energy.

From these estimations, we found important point Q and point S, which divides the symmetry line PΓ in the ratio 3 : 11. In this way, we qualitatively defined the two points as Q = (0, π/a_2) and S = ($22\pi/(21a_1)$, $11\pi/(21a_2)$), as schematically indicated in Scheme 11. In the C_8K complex, the Fermi level goes down very slightly from that of C_6Li, but the points Q and S that we defined for C_6Li can be used for C_8K.

We assume that second-order effects resulting from the occupied and unoccupied two points at Q or at S should play a role for the stacking mode of GICs along with the coulomb interactions between graphite and intercalant layers. To calculate the transition densities at Q and at S, let us look at the important crystal orbitals. The crystal orbitals of bands 1 and 2 at point Q and those of bands 3 and 4 at point S may be written as Eqs. 12, 13, 14, and 15, respectively:

$$|0,\pi/a_2,1\rangle = \frac{1}{\sqrt{N}}\sum_{\nu_1}\sum_{\nu_2}\exp i\pi\nu_2\{\phi_{1,1}(x_1-\nu_1a_1,\, x_2-\nu_2a_2) + \phi_{1,2}(x_1-\nu_1a_1,\, x_2-\nu_2a_2) - \phi_{2,1}(x_1-\nu_1a_1,\, x_2-\nu_2a_2) - \phi_{2,2}(x_1-\nu_1a_1,\, x_2-\nu_2a_2)\} \quad (12)$$

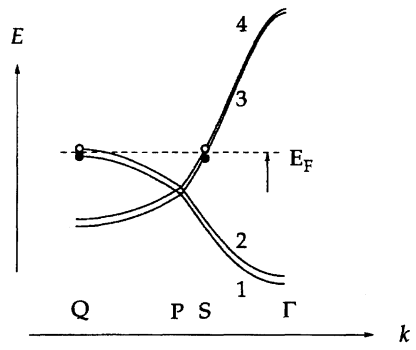

Scheme 11.

$$|0,\pi/a_2,2\rangle = \frac{1}{\sqrt{N}}\sum_{\nu_1}\sum_{\nu_2}\exp i\pi\nu_2\{\phi_{1,1}(x_1-\nu_1a_1,\ x_2-\nu_2a_2) +\phi_{1,2}(x_1-\nu_1a_1,\ x_2-\nu_2a_2)+\phi_{2,1}(x_1-\nu_1a_1,\ x_2-\nu_2a_2) +\phi_{2,2}(x_1-\nu_1a_1,\ x_2-\nu_2a_2)\} \quad (13)$$

$$|22\pi/(21a_1),11\pi/(21a_2),3\rangle = \frac{1}{\sqrt{N}}\sum_{\nu_1}\sum_{\nu_2}\exp \left\{i\left(\frac{22}{21}\pi\nu_1+\frac{11}{21}\pi\nu_2\right)\right\}\{\phi_{1,1}(x_1-\nu_1a_1,\ x_2-\nu_2a_2) -\phi_{1,2}(x_1-\nu_1a_1,\ x_2-\nu_2a_2)-\phi_{2,1}(x_1-\nu_1a_1,\ x_2-\nu_2a_2) +\phi_{2,2}(x_1-\nu_1a_1,\ x_2-\nu_2a_2)\} \quad (14)$$

$$|22\pi/(21a_1),11\pi/(21a_2),4\rangle = \frac{1}{\sqrt{N}}\sum_{\nu_1}\sum_{\nu_2}\exp \left\{i\left(\frac{22}{21}\pi\nu_1+\frac{11}{21}\pi\nu_2\right)\right\}\{\phi_{1,1}(x_1-\nu_1a_1,\ x_2-\nu_2a_2) -\phi_{1,2}(x_1-\nu_1a_1,\ x_2-\nu_2a_2)+\phi_{2,1}(x_1-\nu_1a_1,\ x_2-\nu_2a_2) -\phi_{2,2}(x_1-\nu_1a_1,\ x_2-\nu_2a_2)\} \quad (15)$$

In Fig. 4, we show the crystal orbitals of $|0,\ \pi/a_2,\ 1\rangle$ and $|0,\ \pi/a_2,\ 2\rangle$. The former is occupied and the latter is unoccupied, as mentioned above. It is again important to note that $|0,\ \pi/a_2,\ 1\rangle$ and $|0,\ \pi/a_2,\ 2\rangle$ are in-phase and out-of-phase between the two layers, respectively.

We can calculate the transition densities between the occupied and unoccupied points at Q or at S. The transition density of bands 1 and 2 at point Q may be written as Eq. 16:

$$\langle 0,\pi/a_2,1|\sum_j \delta(r-r_j)|Q_1,\pi/a_2+Q_2,2\rangle = \frac{1}{N}\sum_{\nu_1}\sum_{\nu_2}[\exp(iQ_1a_1\nu_1+iQ_2a_2\nu_2) \times\{(\alpha_{1111}+2\alpha_{1112}+\alpha_{1212}-\alpha_{2121}-2\alpha_{2122}-\alpha_{2222}) +(\beta_{1112}+\beta_{1122}-\beta_{2112}-\beta_{2122}) +\exp(-i\pi)(\gamma_{1112}+\gamma_{1122}-\gamma_{2112}-\gamma_{2122}) +(\beta'_{1211}+\beta'_{1221}-\beta'_{2211}-\beta'_{2221}) +\exp(i\pi)(\gamma'_{1211}+\gamma'_{1221}-\gamma'_{2211}-\gamma'_{2221})\}] \quad (16)$$

And that of bands 3 and 4 at point S is

$$\langle 22\pi/(21a_1),11\pi/(21a_2),3|\sum_j \delta(r-r_j)|22\pi/(21a_1) +Q_1,11\pi/(21a_2)+Q_2,4\rangle = \frac{1}{N}\sum_{\nu_1}\sum_{\nu_2}[\exp(iQ_1a_1\nu_1+iQ_2a_2\nu_2) \times\{(\alpha_{1111}-2\alpha_{1112}+\alpha_{1212}-\alpha_{2121}+2\alpha_{2122}-\alpha_{2222}) +\exp\left(-i\frac{22\pi}{21}\right)(-\beta_{1112}-\beta_{1122}+\beta_{2112}+\beta_{2122}) +\exp\left(-i\frac{11\pi}{21}\right)(-\gamma_{1112}-\gamma_{1122}+\gamma_{2112}+\gamma_{2122}) +\exp\left(i\frac{22\pi}{21}\right)(-\beta'_{1211}-\beta'_{1221}+\beta'_{2211}+\beta'_{2221}) +\exp\left(i\frac{11\pi}{21}\right)(-\gamma'_{1211}-\gamma'_{1221}+\gamma'_{2211}+\gamma'_{2221}\}], \quad (17)$$

where $\alpha_{ijkl}=\phi_{i,j}(x_1-\nu_1a_1,x_2-\nu_2a_2)\phi_{k,l}(x_1-\nu_1a_1,x_2-\nu_2a_2)$ is the intracell overlap within a plane ($i=k$) and between planes ($i\neq k$), and

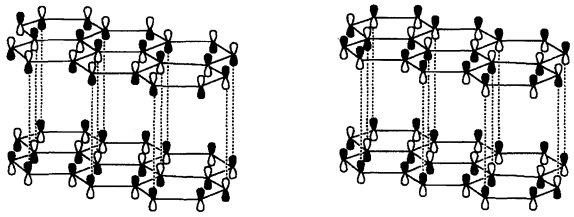

Fig. 4. Crystal orbitals, Eq. 12 (left) and Eq. 13 (right), for a two-layer *AA* stacking model of graphite at point R. The left one is filled and the right one unfilled.

$$\beta_{ijkl}=\phi_{i,j}(x_1-(\nu_1+1)a_1,\ x_2-\nu_2a_2)\phi_{k,l}(x_1-\nu_1a_1,\ x_2-\nu_2a_2),$$
$$\gamma_{ijkl}=\phi_{i,j}(x_1-\nu_1a_1,\ x_2-(\nu_2+1)a_2)\phi_{k,l}(x_1-\nu_1a_1,\ x_2-\nu_2a_2),$$
$$\beta'_{ijkl}=\phi_{i,j}(x_1-(\nu_1-1)a_1,\ x_2-\nu_2a_2)\phi_{k,l}(x_1-\nu_1a_1,\ x_2-\nu_2a_2),$$

and

$$\gamma'_{ijkl}=\phi_{i,j}-(x_1-\nu_1a_1,\ x_2-(\nu_2-1)a_2)\phi_{k,l}(x_1-\nu_1a_1,\ x_2-\nu_2a_2) \quad (i,\ j,\ k,\ l=1 \text{ or } 2)$$

are the corresponding nearest-neighbor intercell overlaps. For example, α_{1122} is the intracell overlap between site 1 of plane 1 and site 2 of plane 2; β_{1122} and γ_{1122} are the intercell overlaps between site 1 of plane 1 and site 2 of plane 2; β'_{1221} and γ'_{1221} are the intercell overlaps between site 2 of plane 1 and site 1 of plane 2, and so on. These examples are indicated schematically in Scheme 12.

We are now interested in the off-diagonal densities in Eqs. 16 and 17. We think that the nearest neighbor basal planes are combined to each other by weak forces from the pσ overlap in the direction of the *c* axis. However, the forces that can cause sliding of graphite layers are not caused by the influence of such vertical forces along the *c* axis. Therefore we have to pay attention to several terms which can slide the layers, such as α_{ijkl}, β_{ijkl}, β'_{ijkl}, γ_{ijkl}, and γ'_{ijkl}, in which $i\neq k$ and $j\neq l$. These terms correspond to off-diagonal densities that are likely to be the main driving forces causing deformation.

Let us first pay attention to the terms of α_{ijkl} in Eq. 16. We can find that there is no net α_{ijkl} ($i\neq k$, $j\neq l$) term that involves the interlayer interactions. We next pay attention to the terms of β_{ijkl} and β'_{ijkl} in Eqs. 16 and 17. We can see that there are β_{1122}, β_{2112}, β'_{1221}, and β'_{2211} terms involved in the interlayer interactions. But these are canceled as:

$$\sum_{\nu_1}\sum_{\nu_2}\{(\beta_{1122}-\beta_{2112})+(\beta'_{1221}-\beta'_{2211})\}=0.$$

Moreover, the terms γ_{1122}, γ_{2112}, γ'_{1221}, and γ'_{2211} are also canceled as shown below:

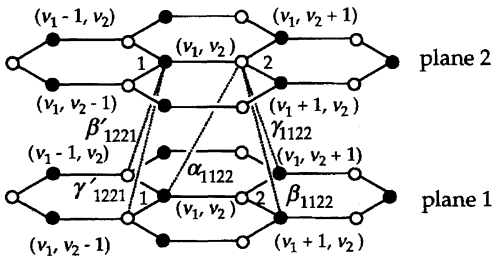

Scheme 12.

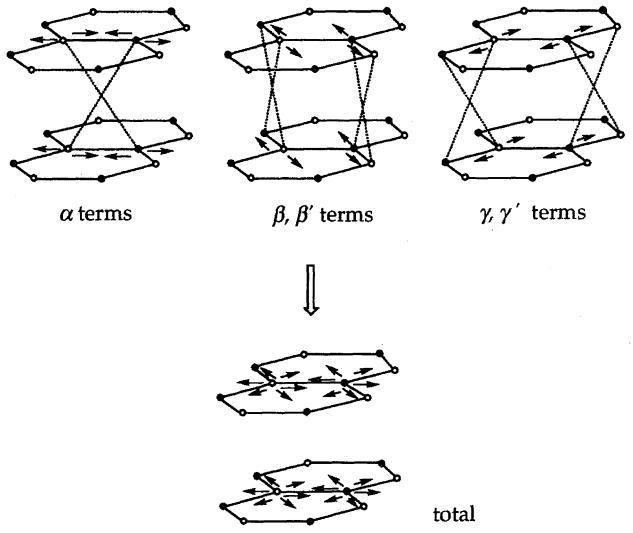

Scheme 13.

$$\sum_{\nu_1}\sum_{\nu_2}\{\exp(-i\pi)(\gamma_{1122}-\gamma_{2112})+\exp(i\pi)(\gamma'_{1221}-\gamma'_{2211})\}=0.$$

As a consequence, we can show schematically in Scheme 13 how the transition densities that cause sliding of layers are canceling each other. This illustration describes an analysis of the transition density of Eq. 16. As in neutral graphite, in Eq. 16 "+" and "−" signify out-of-phase and in-phase interlayer combinations, respectively, because p orbital is antisymmetric in respect of its nodal plane.

The vectors in Scheme 13 show the forces acting on the nuclei, or their preferred motion, due to the electron-distribution relaxation. As can be seen from Scheme 13, these forces are canceling each other, and there remains no net force that can operate on carbon atoms. Thus, the *AAAA* stacking mode in electron-doped graphite is stable against sliding of layers. The other partner (Eq. 17) also has no net forces that can cause the two layers to slide. We can therefore conclude that GICs such as the C_8K and C_6Li complexes take the *AAAA* stacking type because there are no net transition forces operating on carbon atoms in the *AA* stacking mode.

Conclusions

We have investigated from a quantum chemical viewpoint the way that the second-order perturbation functions for the qualitative analysis of interlayer interactions in two-dimensional systems. The interlayer interactions of neutral graphite and GICs have been specifically discussed. The preferred distortions that arise from interlayer interactions have been predicted using an analysis of the transition density near the Fermi level. We have successfully explained the reasons why the well-known *ABAB* stacking of layers in graphite and the *AAAA* stacking of layers in GICs appear. We propose that the interlayer interactions in graphite and GICs should be governed by the orbital interactions in extended systems rather than by the widely believed van der Waals forces.

Our qualitative analysis can be widely applied to the prediction of energetically preferred forms of molecular crystals. One of the reviewers of this paper suggested that it would be interesting to look at various stacking forms of organic molecular conductors from our transition-density analysis.

Table 1. Electrostatic Energies of the *AAAA* and *ABAB* Stackings in GICs

	E_{AAAA} (kcal mol^{-1})	E_{ABAB} (kcal mol^{-1})	ΔE (kcal mol^{-1})
C_6Li[a)]	−207.758	−209.470	1.712
C_8K[b)]	−224.388	−224.596	0.208

a) Energy per $C_{12}Li_2$. b) Energy per $C_{32}K_4$.

This work was supported by a Grant-in-Aid for Scientific Research on Priority Area "Carbon Alloys" from the Ministry of Education, Science and Culture and by "Research for the Future" Program from the Japan Society for the Promotion of Science (JSPS-RFTF96P00206). T. K. is grateful to the Research Fellowships of the JSPS for Young Scientists.

Appendix

The reader of this paper may think that it is obvious that ionic interactions between the layers and the cations should completely dominate the interlayer stacking in GICs. However, we doubt whether only the ionic interactions lead to the *AAAA* stacking of layers in the C_6Li and C_8K complexes. From a qualitative inspection, the *AAAA* structure seems to be unstable from a point of view of electrostatic interactions since the graphite layers and the cations are overlapped completely in this structures. To confirm this, we calculated electrostatic energies of the *AAAA* and *ABAB* stackings in the C_6Li and C_8K complexes. The Ewald summation procedure[29a)] described in a new approach for accelerated convergence by Karasawa and Goddard[41)] was applied to compare the energies, assuming that Li and K atoms have +1 charge and negative charges are distributed equally to C atoms. As shown in Table 1, the *AAAA* stacking of layers is unstable from a viewpoint of electrostatic energy compared with the *ABAB* stacking in the C_6Li and C_8K complexes. The computed energy differences are small, but it is clear that ionic interactions between the layers and the cations cannot explain the real stacking structure in GICs. We thus consider that there are other factors dominating the stacking of layers in GICs except for ionic interactions. Orbital interaction is one of such important factors.

References

1) For example: a) F. A. Cotton and G. Wilkinson, "Advanced Inorganic Chemistry," 4th ed, Wiley, New York (1980); b) J. E. Huheey, E. A. Keiter, and R. L. Keiter, "Inorganic Chemistry," 4th ed, HarperCollins College, New York (1993); c) U. Müller, "Inorganic Structural Chemistry," Wiley, Chichester (1992); d) B. Douglas, D. McDaniel, and J. Alexander, "Concepts and Models of Inorganic Chemistry," 3rd ed, Wiley, New York (1994); e) D. F. Schriver, P. W. Atkins, and C. H. Langford, "Inorganic Chemistry," 2nd ed, Oxford University, Oxford (1995).

2) a) M. S. Dresselhaus and G. Dresselhaus, *Adv. Phys.*, **30**, 139 (1981); b) "Graphite Intercalation Compounds," ed by K. Nakao and S. A. Solin, Elsevier, Lausanne (1985); c) M. S. Dresselhaus, G. Dresselhaus, K. Sugihara, I. L. Spain, and H. A. Goldberg, "Graphite Fibers and Filaments," Springer, Berlin (1988); d) N. B. Brandt, S. M. Chudinov, and Ya. G. Ponomarev, "Semimetals 1. Graphite and Its Compounds," Elsevier, Amsterdam (1988);

e) "Graphite Intercalation Compounds I," ed by H. Zabel and S. A. Solin, Springer, Berlin (1990); f) "Graphite Intercalation Compounds II," ed by H. Zabel and S. A. Solin, Springer, Berlin (1992).

3) J. K. Burdett, "Chemical Bonding in Solids," Oxford University, New York (1995).

4) J. W. McClure, *Carbon*, **7**, 425 (1969).

5) L. Samuelson, I. P. Batra, and C. Roetti, *Solid State Commun.*, **33**, 817 (1980).

6) R. B. Woodward and R. Hoffmann, "The Conservation of Orbital Symmetry," Verlag Chemie, GmbH, Weinheim (1970).

7) K. Fukui, "Theory of Orientation and Stereoselection," Springer-Verlag, Heidelberg (1970).

8) R. G. Pearson, "Symmetry Rules for Chemical Reactions: Orbital Topology and Elementary Processes," Wiley, New York (1976).

9) R. E. Peierls, "Quantum Theory of Solids," Clarendon, Oxford (1955).

10) R. Hoffmann, "Solid and Surfaces: A Chemist's View of Bonding in Extended Structure," VCH, New York (1988).

11) S. Kagoshima, S. H. Nagasawa, and T. Sambongi, "One-Dimensional Conductors," Springer-Verlag, Berlin (1988).

12) S. L. Altmann, "Band Theory of Solids: An Introduction from the Point of View of Symmetry," Oxford University, Oxford (1994).

13) "Charge Density Waves in Solids," ed by L. P. Gor'kov and G. Grüner, Elsevier, Amsterdam (1989).

14) G. Grüner, "Density Waves in Solids," Addison-Wesley, Massachusetts (1994).

15) M.-H. Whangbo, in "Crystal Chemistry and Properties of Materials with Quasi-One-Dimensional Structures," ed by J. Rouxel, Reidel, Dortrecht (1986).

16) M. Kertesz and R. Hoffmann, *Solid State Commun.*, **47**, 97 (1983).

17) T. Hughbanks and R. Hoffmann, *J. Am. Chem. Soc.*, **105**, 3528 (1983).

18) R. A. Wheeler, M.-H. Whangbo, T. Hughbanks, R. Hoffmann, J. K. Burdett, and T. A. Albright, *J. Am. Chem. Soc.*, **108**, 2222 (1986).

19) R. A. Wheeler and P. N. V. P. Kumar, *J. Am. Chem. Soc.*, **114**, 4776 (1992).

20) a) M.-H. Whangbo, *Acc. Chem. Res.*, **16**, 95 (1983); b) *J. Chem. Phys.*, **75**, 4983 (1981).

21) a) J. K. Burdett and J. F. Mitchell, *J. Chem. Phys.*, **102**, 6757 (1995); b) J. F. Mitchell and J. K. Burdett, *J. Chem. Phys.*, **102**, 6762 (1995).

22) Y. Aoki and A. Imamura, *J. Chem. Phys.*, **103**, 9726 (1995).

23) a) R. F. W. Bader, *Mol. Phys.*, **3**, 137 (1960); b) *Can. J. Chem.*, **40**, 1164 (1962).

24) a) R. G. Pearson, *J. Am. Chem. Soc.*, **91**, 4947 (1969); b) *Acc. Chem. Res.*, **4**, 152 (1971).

25) K. Yoshizawa and R. Hoffmann, *J. Chem. Phys.*, **103**, 2126 (1995).

26) K. Yoshizawa, T. Kato, and T. Yamabe, *J. Chem. Phys.*, **105**, 2099 (1996).

27) M. Kertesz and R. Hoffmann, *J. Solid State Chem.*, **54**, 313 (1984).

28) J. P. Lowe, "Quantum Chemistry," 2nd ed, Academic, Boston (1993).

29) a) C. Kittel, "Introduction to Solid State Physics," 6th ed, Wiley, New York (1986); b) N. W. Ashcroft and N. D. Mermin, "Solid State Physics," Saunders, Philadelphia (1976).

30) T. A. Albright, J. K. Burdett, and M.-H. Whangbo, "Orbital Interactions in Chemistry," Wiley, New York (1985).

31) G. Landrum, "YAeHMOP, version 1.0," Cornell University, Ithaca, New York (1995).

32) R. Ramirez and M. C. Böhm, *Int. J. Quantum Chem.*, **30**, 391 (1986).

33) N. A. W. Holzwarth, S. G. Louie, and S. Rabii, *Phys. Rev. B*, **B28**, 1013 (1983).

34) D. Guerard and A. Herold, *Carbon*, **13**, 337 (1975).

35) R. Juza and V. Wehle, *Naturwissenschaften*, **52**, 560 (1965).

36) J. Rossart-Mignod, D. Fruchart, M. J. Moran, J. W. Mulliken, and J. E. Fischer, *Synth. Met.*, **2**, 143 (1980).

37) D. P. DiVincenzo and S. Rabii, *Phys. Rev. B*, **B25**, 4110 (1982).

38) W. Rüdorff and E. Schultze, *Z. Anorg. Chem.*, **277**, 156 (1954).

39) P. LaGrange, D. Guerard, and A. Herold, *Ann. Chim. (Paris)*, **3**, 143 (1978).

40) T. Inoshita, K. Nakao, and H. Kamimura, *J. Phys. Soc. Jpn.*, **43**, 1237 (1977).

41) N. Karasawa and W. A. Goddard, *J. Phys. Chem.*, **93**, 7320 (1989).